







# HOLISTIC LOW-EFFORT MODEL FOR DAMAGE TOLERANCE ANALYSIS IN PRELIMINARY DESIGN

Michael Rohdenburg<sup>1</sup>, Fabian Runge<sup>1,\*</sup>, Matthias Haupt<sup>1</sup>, Lennart Markgraf<sup>2</sup>,  
Peter Horst<sup>1</sup>, Sebastian Heimbs<sup>1</sup>

<sup>1</sup>Technische Universität Braunschweig, Institute of Aircraft Design and Lightweight Structures,  
Hermann-Blenk-Str. 35, 38108 Braunschweig, Germany

<sup>2</sup>IBK Innovation GmbH & Co. KG, Butendeichsweg 2, 21129 Hamburg, Germany

## Abstract

The paper presents reduced order results for three different realistic scenarios with respect to the damage tolerance behaviour. The scenarios are dedicated to stiffened structures and feature the fuselage side panel, the upper fuselage panel and a lower wing panel. A wide range of parameter variations is discussed and the influence on the inspection interval is shown. Results may be used both in preliminary aircraft design and structural optimisation.

**Keywords:** damage tolerance, stiffened structure, reduced order methods

**Type of the work:** research article

## 1. INTRODUCTION

New aircraft concepts, which make use of new, sustainable energy types, will all require low structural mass, owing to density problems in energy storage or energy cost. Such questions have to be checked beforehand in the preliminary design phase to prove feasibility, whether this is in the preliminary concept phase or structural optimisation. One of the obstacles in preliminary design optimisation is the computational effort needed to find reliable results. Therefore, damage tolerance issues are often neglected, although a larger part of the primary structure is sized according to damage tolerance criteria, since they require considerable computational effort, if complex structural items are under scrutiny.

This paper shows a way to provide low-effort damage tolerance results for complex structural items by means of reduced order methods. This is shown by three examples. These basic scenarios are all dedicated to stiffened structures, as these are firstly one of the most relevant in aircraft, and secondly, the effort to calculate residual strength and inspection intervals is considerable. Therefore, reduced effort models are required in preliminary design. The models are *holistic* in the way that they include the influence of many parameters, but since an extremely high number of parameters come up for the scenarios discussed, it has been decided to reduce the dimension of the parameter space by neglecting parameters which proved to be of low impact. Three different typical locations of such structural elements are considered, namely a fuselage side panel, the upper fuselage panel and a lower wing panel. All cases show very different design parameters, e.g., stiffener design and pitch, as well as typical load sequences. The influence of load sequences may be an interesting subject for further

---

This work is licensed under a [Creative Commons Attribution-NonCommercial-NoDerivatives 4.0 International License](https://creativecommons.org/licenses/by-nc-nd/4.0/).

\* Corresponding Author: [fa.runge@tu-braunschweig.de](mailto:fa.runge@tu-braunschweig.de)

investigations, for instance in conjunction with new electronic flight control measures etc. This is not covered in this paper, but the examples show that such influences could be investigated by the method shown, too (see Section 4.3).

The basis of the model is a semi-analytical simulation of cracks in a stiffened structure to evaluate stress intensity factors (SIFs). Based on these factors, crack growth and residual strength may be determined, considering sequence effects via the Wheeler retardation model [1]. Where necessary, the effect of bulging is considered as well. Based on this model, many scenarios are calculated, where many design parameters are systematically varied; this includes material parameters, too. It is still an open point as to whether it is possible to jointly model different material results. Several criteria, e.g., 1-bay and 2-bay cracks, are taken into account. In total, a multi-dimensional matrix of results is found, which may be used to assess damage tolerance behaviour of structures in preliminary design.

Several semi-numerical models have been developed over the years. Early versions date back as far as the 60s. Well-known is the one by Poe [2], which already includes the main ideas behind the current models. The model used to evaluate SIFs in this paper was proposed by Nishimura [3]. Correction factors for bulging in pressurised stiffened structures have been shown by Chen [4]. There exists a vast literature on preliminary aircraft design optimisation as well as structural optimisation. Preliminary or conceptual aircraft design ranges from statistical based methods for instance [5] to physically based methods for the different disciplines [6]. But even the highly sophisticated physically based methods do not include fatigue and damage tolerance issues due to the high computational effort. Structural optimisation is a widely developed area with many special directions of special interest [7]; but even very sophisticated ones such as Hansen and Horst [8] do not include damage tolerance in depth, but use for instance allowable stresses at 1 g instead, which is a very coarse way to do it. Several methods to reduce models exist, as well as software tools to facilitate them. A few points concerning such tools are given in Section 3.5. In literature also, some sources are found dealing with reduced order models for crack propagation issues [9]. What is not found are cases where the applied problem of damage tolerance with a combination of criteria is handled.

## 2. SCENARIOS

The paper discusses three basic scenarios, all covering typical *principle structural elements*, and likely to trigger the structural sizing of aircraft substantially, especially with regard to damage tolerance requirements. They are therefore quite suitable to serve as examples acting as input for later use in structural optimisation or sizing in conceptual design studies. The three scenarios are (see Fig. 1):

- Scenario 1: longitudinal fuselage crack (e.g., in a side panel)
- Scenario 2: circumferential crack in the crown area of a fuselage
- Scenario 3: chordwise crack in the lower wing panel

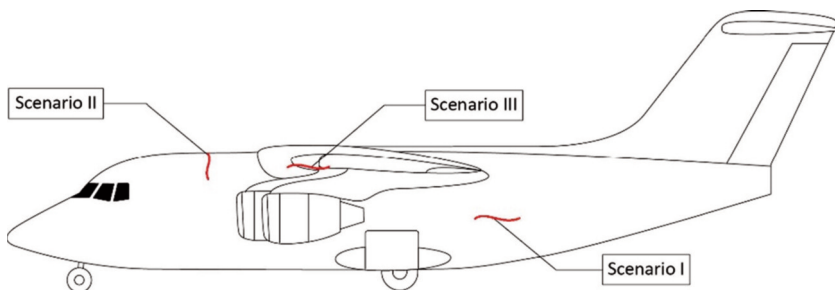


Figure 1. Location of the three scenarios.

All scenarios feature stiffened structures, as they are usual in transport aircraft. In this paper only differential stiffener designs are discussed, but this does not limit the applicability of the calculation method; indeed it could easily be extended to integrally stiffened designs [10–12]. One crucial characteristic of the three different scenarios is the very dissimilar type of load histories to be expected. This was one of the questions raised by the project partners. While Scenario 1 will feature nearly constant amplitude loading, Scenario 2 is characterised by a ground-air-ground (GAG) cycle, and Scenario 3 is a good example of variable amplitude loading, where retardation plays a key role.

Furthermore, the three scenarios differ considerably in the parameters specifying stiffening of the panels. While in Scenario 1 typical frame pitches are usually in the order of  $\geq 500$  mm, typical stringer pitches in the fuselage crown area are in the order of 200 mm. Stringer pitches in lower wing panels are usually quite small compared to the fuselage case. In addition, also the stiffener/skin area ratio is relatively low for the first two scenarios compared to the third case [for definition, see Eq. (1)].

Apart from the stiffener pitch  $b_s$  in Fig. 2, many further parameters have to be specified, and form to a certain extent the possible dimensions of response surfaces or input of neural networks. Apart from those depicted in Fig. 2, there are the Young’s modulus of skin and stiffeners, rivet diameter, cracked or uncracked central stiffener and the loading of the stiffeners  $\sigma_s$  – but also parameters such as the fuselage radius  $R_f$  which has to be distinguished from the stress ratio  $R$  in case of Scenario 1. A rivet diameter of 4 mm and a rivet spacing of  $y_s = 20$  mm are used throughout the following calculations. To reduce the parameters discussed in this paper,  $\sigma_p$  and  $\sigma_s$  are assumed to be equal and are referred to as  $\sigma$  in the following.

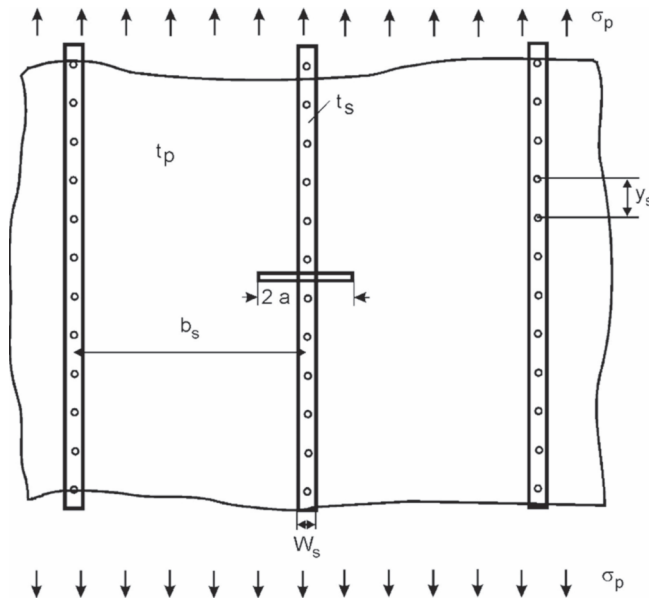


Figure 2. Stiffened panel modelling parameters ( $\sigma_p$  – remote stress in the plate,  $t_p$  – plate thickness,  $t_s$  – stiffener thickness,  $W_s$  – stiffener width,  $b_s$  – stiffener pitch,  $a$  – half crack length,  $y_s$  – rivet pitch); stringer and plate with Young’s modulus  $E_s$  and  $E_p$ , respectively.

All cases considered here are single crack cases. Multiple site damage is not covered. Apart from the case of a central crack under an intact or broken stiffener, the case of a central crack between two intact stiffeners is accounted for. The case of a continuously cracking stiffener has not been considered in this paper. The stiffener ratio is defined by

$$q_s = \frac{W_s t_s E_s}{b_s t_p E_p}. \quad (1)$$

This definition may differ from some used in industry, but it is very clear for this case. Without loss of generality, standard 2024 T3 aluminium alloy has been used throughout this paper.

### 2.1. Scenario 1: longitudinal fuselage crack

From a loads point of view Scenario 1 is extremely simple; as mentioned above, it is pure constant amplitude loading at a stress ratio  $R = 0$ . Nevertheless, this scenario is often essential for the minimum skin thickness sizing in conjunction with frame dimensions and pitch. Both, crack growth and critical length, are of interest, as well as the integrity of the stiffeners. Since at least the frame pitch is usually kept constant along a given fuselage, this scenario is of global interest for the design, particularly in the overall design optimisation.

Loading is completely based on hoop stress  $\sigma_p$  from internal pressure differential  $\Delta p$  [Eq. (2)] and the stress increase between frames due to bulging (see Section 3.4). The influence of the frames may be accounted for by well-known equations from Flügge [13] or detailed finite element simulations.

$$\sigma = \Delta p \cdot \frac{R_f}{t_p} \quad (2)$$

Where not stated otherwise, in this paper the parameter values given in Table 1 have been used in Scenario 1 simulations.

Table 1. Parameter intervals Scenario 1.

Parameter	Interval	Unit
$b_s$	500–650	mm
$t_p b_s / W_s t_s$	0.1–0.3	–
$\sigma$	80–120	MPa
$p$	0.057	MPa
$R$	0.0	–
Limit load	1.15	MPa
$a_{det}$	37.5	mm

### 2.2. Scenario 2: circumferential crack in the crown area of a fuselage

Scenario 2 bears a more complex load sequence. GAG cycles of the fuselage crown area primarily include three parts: First, the part owing to internal pressure, i.e., half the hoop stress. Second, normal stress from fuselage bending under 1 g-loading, where the amount will heavily depend on the distance of the actual damage site from the responsible main frame. In addition, loads from vertical gust or manoeuvre are playing a role (see for instance the well-known report by Broek [14]). A typical load history as used for Scenario 2 is shown in Fig. 3a.

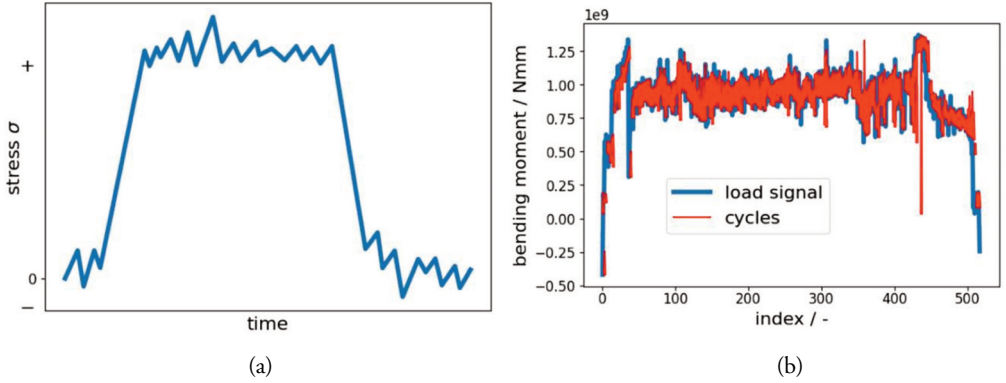


Figure 3. GAG cycles. (a) Typical load history for Scenario 2. (b) Load history for Scenario 3.

For the determination of the normal stresses for Scenario 2 an approach has been adopted based on the procedure in Broek et al. [14] and RAPID Manual [15]. Firstly, acceleration levels for the centre of gravity during pre-flight taxiing, climb, cruise, descent, landing impact and post-flight taxiing have been taken from RAPID Manual [15], and these have been obtained from NASA measurements [16]. Accelerations due to vertical gusts are determined by calculating the change in lift  $\Delta L$  due to the vertical gust speed  $w_g$  via

$$\Delta L = \frac{\rho}{2} V^2 S \frac{dC_L}{d\alpha} \frac{w_g - w(t)}{V} \quad (3)$$

with the air density  $\rho$ , flight speed  $V$ , reference area  $S$ , the global lift coefficient  $C_L$ , the angle of attack  $\alpha$  and the velocity of the airplane  $w(t)$  due to the vertical gust. Generally, a gust alleviation factor

$$K_g(t) = \frac{w_g - w(t)}{w_g} \quad (4)$$

may be introduced into Eq. (3); see Gudmundsson [17]. The gust alleviation factor accounts for the fact that the change in lift does not happen instantly. Here the conservative case is assumed, by setting  $w(t)$  to zero. With known parameters of an aircraft configuration during the preliminary design phase, e.g., operating aircraft mass, fuel mass, flight height and geometrical information (such as fuselage radius, fuselage, reference area and landing gear positions), the bending moment of the fuselage for an arbitrary crack location along the longitudinal axis of the fuselage is calculated for a BAE 146-like configuration. The mass distribution is assumed to be constant for the fuselage in front of and behind the wing. Depending on the data provided within the preliminary design, the mass distribution could be modelled more accurately resulting in a more realistic bending moment  $M_b$ . By utilising typical design parameters for Scenario 2, e.g., skin thickness, stringer thickness and pitch, see Table 2, the second moment of area  $I$  for a simplified fuselage section is obtained for the calculation of the bending stress. The loads are assumed to be stationary (as in Broek et al. [14]), i.e., the acceleration levels cause a stationary bending line of the fuselage. Table 2 summarises the data used for the calculations.

Table 2. Parameter intervals Scenario 2.

Parameter	Interval	Unit
$b_s$	100.0–250.0	mm
$t_p$	1.0–3.0	mm
$t_s/t_p$	1.0–1.5	–
$\sigma$	GAG	MPa
$R$	GAG	–
$a_{det}$	37.5	mm
$W_s$	10.0	mm

This scenario is often responsible for sizing of the crown area of fuselages, and therefore it makes sense to include it here. Clearly, the load sequence will have an impact on the crack propagation, although it may not be as pronounced as in Scenario 3.

### 2.3. Scenario 3: chordwise crack in the lower wing panel

In contrast to the fuselage with a high inertia and a pressurisation leading to similar mean stresses each flight, wing loads are very well-known for highly variable amplitude sequences. Therefore, it makes sense to look more closely at these and to take retardation into account. In addition, skin thickness is usually much higher in the wing root area than at the fuselage. Parameters used in the calculations are summarised in Table 2.

To account for the very dynamic behaviour of the wing, load calculation for the wing is not solely based on centre of gravity measurements in contrast to Scenario 2. Hence the GAG cycle used here for the wing root of the lower panel is obtained from a load estimator. The load estimator was developed and applied in the frame of the German Luftfahrtforschungsprogramm (LuFo) project OMAHA by IBK-Innovation GmbH & Co. together with the DLR Oberpfaffenhofen in the context of load alleviation functions. The estimator splits up into two components. Firstly, an estimator for the inertial load increment based on corresponding formulas and look-up tables covering rigid body motion. Secondly, an estimator for the aerodynamic load increment as well as loads due to flexibility effects based on an Adaptive-Network-based Fuzzy Inference System (ANFIS) [18]. In this type of network, a set of so-called fuzzy rules is applied to perform a non-linear interpolation between multiple local approximations (least-square). For training of the ANFIS model a large set of trim simulations is used, which are chosen in a way that the room of hyper-parameters (angle of attack, body rates, Mach number, etc.) is well covered. In the investigations, the trim simulations have been performed for the JTI-XRF1 model, which is a theoretical aircraft model provided by AIRBUS. For damage tolerance analyses shown here, only a single flight from the in-service recordings of a regional jet is used [19]. (The recordings contain data of commercial service over a 3-year period for a single jet type, but are not utilised here.) The flight duration is 4.5 h. The flight regime of the two different aircraft is adapted by scaling factors on the Mach number and the dynamic pressure, and a load scaling is realised via the ratio of the masses (maximum take-off weight) for the inertial load increment and the ratio of the wing reference areas for the aerodynamic contribution.

The wing root bending moment used for the calculation of the bending stresses for Scenario 3 is shown in Fig. 3b. The second moment of area is  $I$  calculated for a simplified rectangular 2-spar wing box with a width of 2,500 mm and height of 580 mm. The bending moment history is explained by changes in climb rates, manoeuvres and gusts. Ground loads are not included in the GAG cycle. However, an average ground case usually will not cause significant crack growth, because the mean stress of the lower wing panel on the ground is negative (pressure). Additionally, crack growth due to ground loads is slowed down due to retardation effects caused by the tension stress from the flight phase.

Table 3. Parameter intervals Scenario 3.

Parameter	Interval	Unit
$b_s$	80.0–150.0	mm
$t_p$	6.0–10.0	mm
$t_s/t_p$	1.0–1.5	–
$\sigma$	GAG	MPa
$R$	GAG	–
$a_{det}$	37.5	mm
$W_s$	10.0	mm

## 2.4 Criteria

Many variables may be used to represent results of the calculations and in turn, the output of the response surface or neural network models. With respect to the use in optimisation loops, it seems to be realistic to use two types of data, first, the inspection interval and second, the critical crack length (or the critical stress for a given crack length).

The inspection interval is defined in the way that the number of flight cycles between a defined detectable half crack length  $a_{det}$  and the critical half crack length during crack growth is divided by a scatter factor. In this paper a scatter factor of 2 is utilised. A different one may be used instead, but this would not alter the character of the results.

The critical crack length is evaluated by means of comparison of the critical SIF  $K_c$  and the current maximum stress, which depends on the thickness. Making an assumption for the expectable limit load and comparing against it would decrease the calculated inspection intervals shown in the following. However, this does not change the relationship of the results among each other because the stress at limit load is again a function of the thickness, i.e., a thicker structure will still have a lower stress at limit load, which is the same relationship as in the approach chosen here. Refer to Section 3 for the calculation of the crack growth.

Since stiffened structures are investigated here, it is necessary to specify which type of residual strength requirement is used. In all cases it is required that the residual strength is high enough to allow that the crack tips will reach the next intact stiffeners. This means that for cases with a central crack between two intact stiffeners a so-called 1-bay-crack criterion is used, while for cases where a central crack is located under an intact or cracked stiffener, a 2-bay-crack criterion is used (which is of course much harder to reach). This second case is shown in Fig. 2. The question which criterion is applied may be subject to discussions.

An example may illustrate typical data. Figure 4 presents crack growth curves for a Scenario 1 case, where the crack is located under a central frame. The frame pitch  $b_s$  is 520 mm, and frame width and thickness are 30 mm and 4 mm, respectively. The skin panel thickness  $t_p$  is 2 mm, and the fuselage pressure differential  $\Delta p$  is 0 MPa at ground level and 0.057 MPa in flight, leading to corresponding hoop stresses. Figure 4 shows three bundles of crack growth curves, which are related to three different fuselage radii, and each include the effect of changing Young's moduli. The right-hand bundle ( $R_f = 1,800$  mm) exhibits a typical bend in the curves, indicating the influence of the adjacent frames (shown as grey line). When the crack tip reaches the vicinity of the frames, crack growth slows down. In the case of the two left-hand bundles, crack growth becomes so fast, that a critical situation is reached before the next frames are reached. Hence, these are cases where the 2-bay crack criterion is not fulfilled.

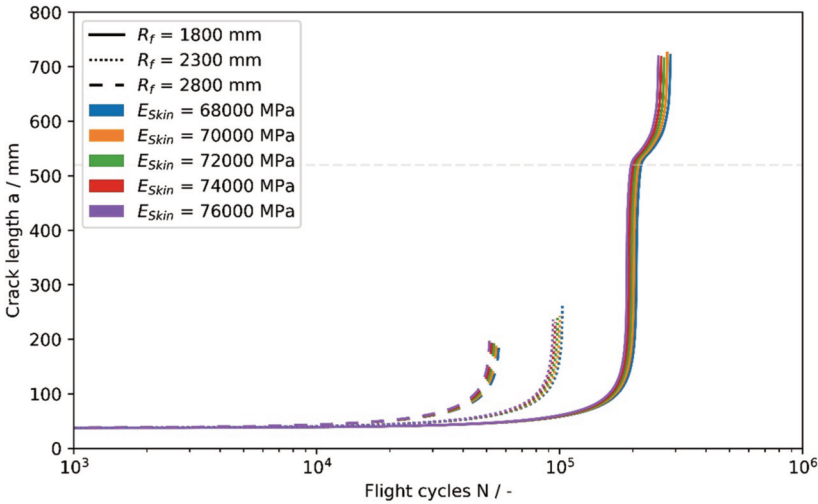


Figure 4. Crack growth curves for Scenario 1, where  $b_s = 520$  mm,  $q_s = 0.115$ ,  $t_p = 2$  mm and  $\Delta p = 0.057$  MPa.

### 3. DAMAGE TOLERANCE MODEL

#### 3.1 Stress intensity factors

Damage tolerance behaviour is calculated throughout this paper based on SIFs; these consist of the applied stress  $\sigma$ , the half crack length  $a$  and a correction factor  $\beta$  as standard

$$K = \sigma \beta \sqrt{\pi a}. \quad (5)$$

The correction factor  $\beta = \beta_0, \beta_1, \dots$  describes geometrical conditions as well as technical conditions originating, e.g., from manufacturing. To calculate crack growth induced by cyclic loading, a simple but nowadays widely used model was proposed by Forman [20], considering the stress ratio  $R$ :

$$\frac{da}{dN} = \frac{C \cdot \Delta K^m}{(1-R)K_c - \Delta K} \quad (6)$$

where  $N$  is the number of cycles and  $C$  and  $m$  are material parameters estimated by regression of test measurements for constant amplitude loading.



### 3.2. SIFs for stiffened structures

A suitable calculation method for SIFs of cracks in stiffened panels is required so that crack growth and critical crack length may be calculated. The stiffeners usually have a retarding effect on the crack growth and also increase the residual strength for cases where the crack tip is in the vicinity of the stiffeners. The semi-analytical SIF calculation method suggested by Nishimura [3] is used, which is based on compatible displacements between the sheet, stiffener and rivets. The displacement at point  $i$  of the plate

$$v_{p,i} = -\sum_j A_{ij} Q_j^u + B_i \sigma \quad (7)$$

and point  $i$  of the stringer

$$v_i^s = \sum_j A_{i,j}^s Q_j^u + B_i^s \frac{E_s}{E_p} \sigma \quad (8)$$

depends on the remote stress  $\sigma$  and the unit rivet force  $Q_j^u$  at point  $j$  [2].  $A_{ij}$  and  $A_{ij}^s$  are displacement contributions due to rivet forces in the plate and in the stringer, where the superscript  $s$  indicates the stringer.  $B_i$  and  $B_i^s$  represent displacements contributions due to remote stress. By requiring  $i$  compatible displacements, a dense linear system of equations is formulated for a truncated number of rivets

$$\sum_j (A_{ij} + A_{ij}^s) Q_j - \left( B_i - \frac{E_s}{E_p} B_i^s \right) \sigma = 0 \quad (9)$$

that can be solved for the unknown rivet forces  $Q_j$ , which is key for the determination of the SIF. Preliminary studies to identify an appropriate number of truncated rivets have shown that 20 rivets per stiffener are sufficient for the SIF calculation throughout the crack growth calculation in order not to extend the computational effort. The semi-analytical model provides a way for relatively fast computation of the SIFs, which is useful for parametric studies with many design variables, as needed in this study. But, first, it could be extended to more complex models and second, this model also needs computational effort owing to the high number of recalculations of the a.m. system of equations. The model assumes linear elastic material behaviour. An exemplary crack scenario is shown in Fig. 2. The uniaxial remote stress acts perpendicular to the crack growth. Changes in crack growth directions due to mixed mode loading are not considered. The stress acts in the middle plane of the sheet and stiffeners, i.e., that bending stiffness is zero, although the effect of the eccentricity of the stiffeners could be accounted for with methods proposed, e.g., by Swift [21].

### 3.3 Retardation

For variable amplitude stress histories, as experienced during aircraft operation, load interactions play an important role when investigating crack growth behaviour. An overload in the load sequence of a metallic component may have a positive effect on the remaining usage life (RUL), which is known as retardation. The crack growth rate is increased for the overload cycle itself, but the subsequent crack growth is decelerated due to the overload. The relatively simple Wheeler retardation model [1] has been applied in this paper; it assumes that residual stresses in front of the crack tip are responsible for the retardation effect [22]. A retardation factor

$$C_p = \left( \frac{r_c}{a_o + r_o - a_c} \right) \quad (10)$$

is calculated from the crack size  $a_o$  and plastic zone size  $r_o$  at the overload with the current crack size  $a_c$  and the plastic zone size  $r_c$ .  $m_w$  is an empirical retardation exponent that depends on the spectrum [23]. The retardation exponent is defined as  $m_w = 1$  for all calculations in this paper, because choosing  $m_w$  with respect to the spectrum does not change the character of the results. According to the Wheeler model, the retardation is highest directly after the overload. The retardation effect diminishes when the crack grows within the plastic zone and vanishes as soon as the crack tip has grown out of the plastic zone. More sophisticated models are available, but their usage here would exceed the limitations of the paper.

### 3.4 Bulging

In pressurised vessels, the internal pressure acting on crack edges results in out-of-plane deformation, so-called bulging.

This causes higher effective SIFs for longitudinal cracks, and in turn higher crack growth rates. To account for this, the bulging factor  $\beta_b$  is introduced. A minimum value of this factor equal to 1.0 is assumed at frame positions, as the frame presumably mitigates bulging, and takes its maximum value between two frames. It has been shown by Chen [4] that Eqs (11) and (12) agree well with finite element results for aircraft structures.

$$\beta_{b,1bay} = \sqrt{1 + \frac{5}{6\pi} \frac{E_p t_p a}{R_f^2 \Delta p} \frac{1}{\sqrt{180\chi + 10}} \tanh \left( 0.06 \frac{R_f}{t_p} \sqrt{\frac{\Delta p a}{E_p t_p}} \right) \left( 1 + \cos \frac{2\pi a}{b_s} \right)} \quad (11)$$

$$\beta_{b,2bay} = \sqrt{1 + \frac{5}{6\pi} \frac{E_p t_p \frac{b_s}{4}}{R_f^2 \Delta p} \frac{1}{\sqrt{180\chi + 10}} \tanh \left( 0.06 \frac{R_f}{t_p} \sqrt{\frac{\Delta p b_s}{4E_p t_p}} \right) \left( 1 + \cos \left( \pi \left( 1 - \frac{4a}{b_s} \right) \right) \right)} \quad (12)$$

### 3.5 Response surface methodology (RSM)

As the simulation runtime is quite large from a preliminary design optimisation point of view, measures have to be taken to reduce computational effort. One approach is omitting the costly recalculation of SIFs where feasible, e.g., at the beginning, when crack growth is small. This improves runtimes considerably. Nevertheless, the 6,545 simulations conducted to create Fig. 5 take approximately 1 h to calculate in parallel on 20 cores for this simple scenario. To reduce calculation time to a minimum, response surfaces are utilised. These model the relationship of input variables to output variables based on prior simulations, trading computing time for accuracy. Several variables could be modelled by such RSM. The two main points of interest chosen here are firstly the admissibility of the configuration (e.g., via the 2-bay-crack criterion) and secondly the load cycles endured. The admission of a configuration is a classification problem, which can be modelled, e.g., via support vector classification (SVC). As the decision surface is non-linear, a radial basis function (RBF) kernel is chosen. Predicting the load cycles endured is a regression problem, as a continuous response to input parameters is to be found. This can be modelled with, e.g., a linear regression, even though the response surface is again non-linear. For this the polynomial features – mixed as well as higher order terms – have to be substituted, yielding a multivariate linear regression for each parameter. To mitigate skewed results due to the big differences

in input parameter scales, the substituted parameters are normalised after the fact. In all response surface studies in this paper the implementations of scikit-learn 0.24.2 [24] have been used.

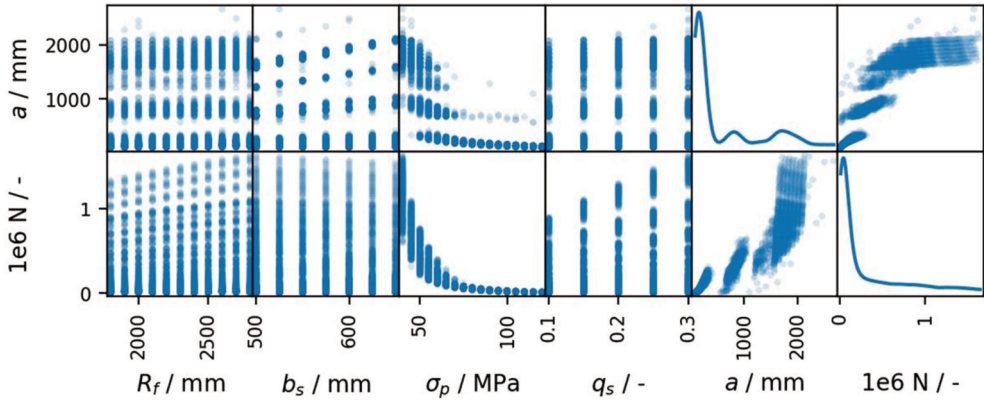


Figure 5. Scatter plot matrix showing parameter relationships, Scenario 1.

## 4. RESULTS

The results for the three a.m. scenarios are discussed in the forthcoming sub-sections.

### 4.1 Scenario 1

As mentioned already in the introduction, it makes sense to carry out some kind of importance sampling in order to reduce the number of dimensions of parameter space. In Fig. 5 all simulations runs for Scenario 1 are represented by a dot, showing the influence of each parameter on half crack length ( $a$ ) and load cycles endured ( $LC$ ). This scatter plot matrix may be used to decide on parameter importance. By far the most important parameter is the hoop stress, which has large impact on crack length as well as load cycles endured. As is to be expected, the less stress is applied to the structure, the more cycles can be endured. Less of an impact on crack length but on load cycles have the fuselage radius and the stiffener ratio (see Fig. 8 for details). In turn, the frame pitch has little impact on load cycles, whereas crack lengths can be higher with larger frame pitch. From the whitespace around frame positions in all crack length diagrams (upper row Fig. 5) it can be seen that critical crack growth is not reached in the vicinity of frames. This implicitly also shows the simulations not fulfilling the 2-bay-crack criterion. As the two density plots show, most of the simulated parameter combinations do not.

To capture the above classification observations, the SVC model introduced in Section 3.5 is trained using the presented data. The predicted probability of admission  $P$  regarding the 2-bay-crack criterion is shown in Fig. 6, the simulation values ('ground truth') are superimposed in red. The decision surface is shown as a black line. Although only an exemplary section at  $q_s = 0.2$  and  $\sigma = 60$  MPa is shown for reasons of available space in this paper, the whole parameter space is modelled and can be viewed alike. Testing the model on a testing dataset not included in the training dataset, the mean prediction accuracy is approximately 99%. Likewise, admission predictions according to an inspection interval criterion are possible. Figure 7 shows the admission probability as before, but for an inspection interval of 16,000 cycles (already factoring in the scatter factor). This criterion is fulfilled even at comparatively high hoop stress. The graphs display the decision surface at  $\sigma = 110$  MPa with varying stiffener ratios  $q_s$ . The mean prediction accuracy for this use case is approximately 99% as well. From the boundary regions shown it is clear that the accuracy of the model deteriorates at parameter space boundaries.

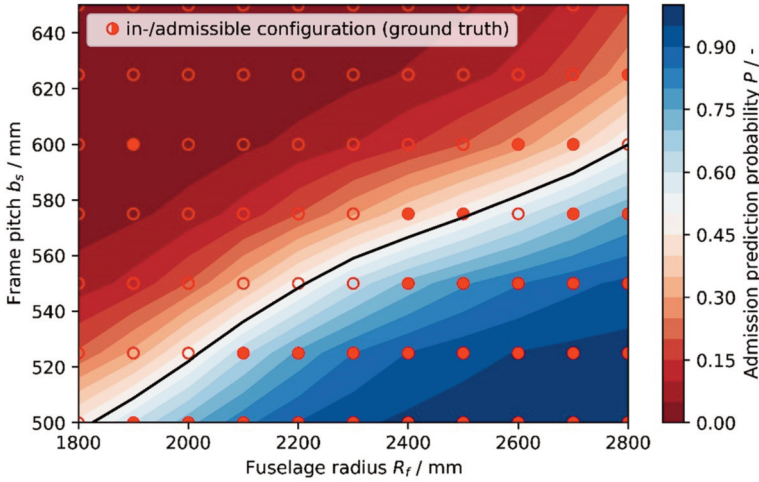


Figure 6. 2-bay-crack criterion: Admission probability  $P$  for Scenario 1 at  $q_s = 0.2$  and  $\sigma = 60$  MPa, simulation values ‘ground truth’ superimposed in red, filled circles indicating admissible configurations, decision surface in black.

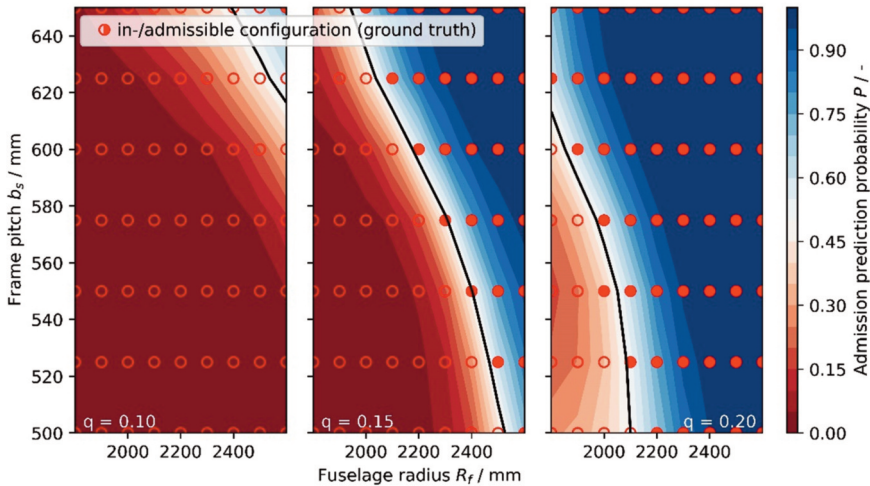


Figure 7. Inspection interval criterion: Admission probability  $P$  for Scenario 1 at  $\sigma = 110$  MPa, simulation values ‘ground truth’ superimposed in red, filled circles indicating admissible configurations enduring 16,000 cycles, decision surface in black.

An optimisation for accuracy in this regard is subject to further research, e.g., using points outside the parameter space of interest for training data (cf. central composite circumscribed design of experiment). Regression of crack lengths or load cycles endured is more complicated. From Fig. 4 it can be imagined that each frame in the crack path results in a similar bend in the curves to the one shown, yielding a smooth stepped function. This means that while cracks reaching no frame at all could be approximated by a function of degree two, the necessary degree for one frame would be five already. Unfortunately, higher degree polynomials do not automatically translate to higher accuracy on large  $da/dN$  values or better resolution of the steps. Tests have shown that an accuracy of approximately 95% can be achieved, although the steps are averaged out and thus not reproduced correctly. Rather than

trying to fit a single high degree function to the complete dataset, the classification approach above is extended to yield the frame number the crack has reached as presented in Fig. 8.

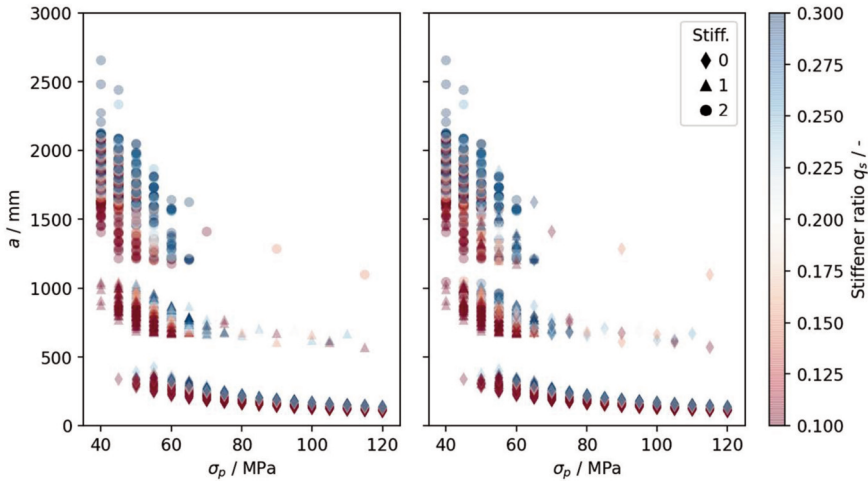


Figure 8. Crack length at failure in dependence of hoop stress  $\sigma$  and stiffener ratio  $q_s$ , clustering (left) vs. classification (right) of results by stiffeners reached by crack.

This information is adopted to decide which regression function is used to estimate the parameter of interest. The clusters (left) show the frames reached by analysing the crack length on the simulation data. The classification (right) shows the number of frames reached as predicted by SVC. The boundaries of the parameter subspaces are still not predicted accurately (e.g., around  $\sigma = 55$  MPa,  $a = 1,000$  mm). Moreover, most of the outliers are not predicted correctly. These can be attributed to calculation parameters such as step size and can be mitigated, entailing increased calculation times. It is expected that cycle-by-cycle results of these outliers will be more in line with the classification prediction. Despite these observations, the classification accuracy is approximately 97%. Polynomials of degree three have been shown to approximate endured cycles for the first frame sub-space with approximately 98%. This leads to an overall accuracy of this approach of 95% as well, while maintaining a better representation of plateaus and better scalability. For future research, the prediction pipeline parts used in the latter approach will be unified via Gaussian Mixture Regression. A (dis-/continuous) spline (e.g., Non-Uniform Rational B-Splines) approach is conceivable as well. The stress in the stiffeners is not checked for Scenario 1. While this does not affect the accuracy of predictions of the RSM, it does lead to unrealistically high crack lengths, see Figs 5 and 8. By enabling the check, this is eliminated for Scenario 2 and 3.

## 4.2 Scenario 2

The data used for the load spectrum generation has been taken from centre of gravity measurements for a narrow wing body configuration, as described in Section 2.2. One single spectrum corresponds to the loading of a 1.5 h flight. A lifetime of 60,000 flight hours has been assumed, which is equivalent to 40,000 flights for the investigations done for Scenario 2. The aim for aircraft design in general is a maximum utilisation of the structure without risking failure of operation critical components. Therefore, results which indicate a higher inspection interval than 40,000 flights reveal a low material utilisation from a damage tolerance perspective, i.e., structural mass could be removed, which would make the aircraft lighter and more efficient.

Important design variables during the preliminary design phase are stringer pitch  $b_s$ , skin thickness  $t_p$  and stringer thickness  $t_s$ , which have a high influence on the overall aircraft mass. Therefore, the influence of these design variables on the inspection interval is of interest. In Fig. 9 each red circle corresponds to a cycle by cycle crack growth simulation including retardation. The crack location is indicated by the dimensionless coordinate  $\xi$ , where  $\xi = 0$  and  $\xi = 1$  refer to a position close to the nose landing gear and in front of the wing, respectively. The parameter combination is illustrated as admissible when the crack has reached at least one stringer. The black threshold line surrounds all inadmissible results. Fig. 9a shows that it is much easier for a 1-bay crack to reach the first stiffener than for a 2-bay crack, because the distance from the crack tip to the next stiffener is always smaller than  $b_s/2$  ( $b_s$  for 2-bay cracks). Therefore, the inspection interval drops significantly for 2-bay-cracks, see Fig. 9b, and most results are inadmissible at the unconventionally low skin thickness of  $t_p = 2.0$  mm, except when using very small stringer pitches  $b_s$ . An intact central stringer slows down crack growth, so that the inspection interval is increased, but usually cannot reduce the SIF enough to prevent critical crack growth before reaching the stringer. Thus, the admissibility of the results is unchanged.

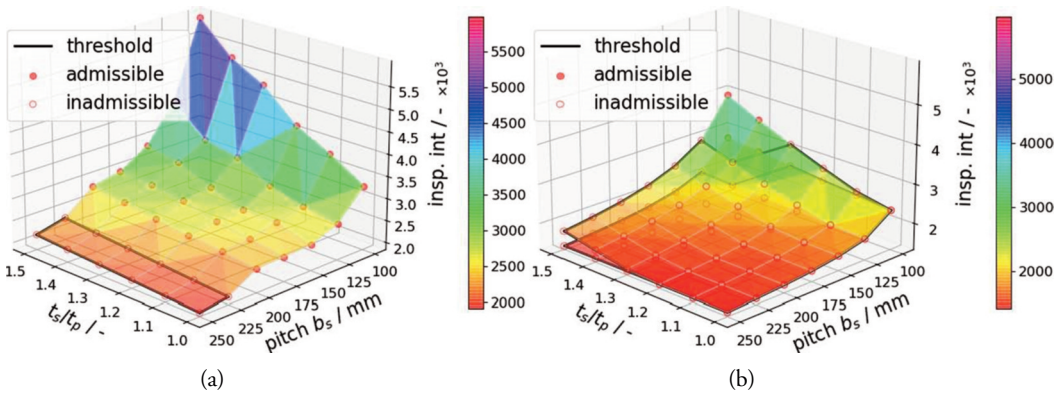


Figure 9. Comparison of 1- and 2-bay-cracks for Scenario 2 at  $\xi = 1.0$ ,  $t_p = 2.0$  mm. (a) 1-bay-crack and (b) 2-bay-crack with intact/broken central stringer.

Figure 10 shows that close to the wing, skin thicknesses above  $t_p = 2.5$  mm are required to obtain admissible configurations for a variety of  $b_s$ . For  $t_p = 3.0$  mm the inspection interval has increased to well above 10,000, i.e., one-quarter of the assumed aircraft lifetime. The notable differences between  $t_p$  is mainly due to the increase of  $I$ , which decreases the applied stress  $\sigma$ . A decreasing pitch  $b_s$  (more densely spaced stiffeners) increases  $I$  as well. The second stringer (from the view point of the crack tip) is only reached for  $b_s$  100 mm at  $t_p = 3.0$  mm. The influence of single parameter variations on the inspection interval is shown in Fig. 11 for the 1-bay and 2-bay case. The parameters used for the calculations are indicated by the bold abscissa value. For Fig. 11A some parameters cause high inspection intervals, which are not included in the figure. Due to the assumed stationary bending of the fuselage, see Section 2.2, the stress change is non-linear when varying the crack location, which makes the crack location an important parameter. The investigated factors in Fig. 11B are scaling factors of the original stresses associated with gust, manoeuvre, etc. as calculated from the GAG cycle. The inspection interval for a gust factor of 0.7 is higher than for a gust factor of 0.6. This is due to the retardation effect, which is governed by the maximum stress in the GAG cycle. For very high gust factors above 1.5, the potential for load alleviation mechanisms is of interest. The manoeuvre factor curves also emphasise the importance of operation at slow turn rates. The contribution of the landing factor is negligible here because the GAG cycle only features mean load measurements with low loads due to landing. Reverse plasticity effects are not considered within the Wheeler retardation model applied here. In reality, the compressive stresses

(upwards bending of the fuselage) due to landing loads have a negative impact on the fatigue life. Furthermore, the landing loads occur shortly after the overload due to the gust, i.e., crack growth is very slow. The pressure difference of 0.57 bar corresponds to a factor  $\Delta p = 1$  for the fuselage cabin. The variation of  $\Delta p$  is interesting, e.g., when the airline wants to change the pressure in the fuselage cabin for cost reductions or improvement of the cabin comfort while retaining the flight height. A promising method for the reduction of climate effects due to aircraft traffic is climate optimised routing. The climate effect due to non-CO<sub>2</sub> emissions depend on the location and altitude of the emission [25]. Adapting the flight height of about 600 m to avoid formation of contrails is suggested in Schumann et al. [26]. This would require additional manoeuvres and would lead to changes in  $\Delta p$  of about 5%. The flight height is also relevant because it increases the stress ratio  $R$ . Thus, crack growth is accelerated because crack closure is aggravated.

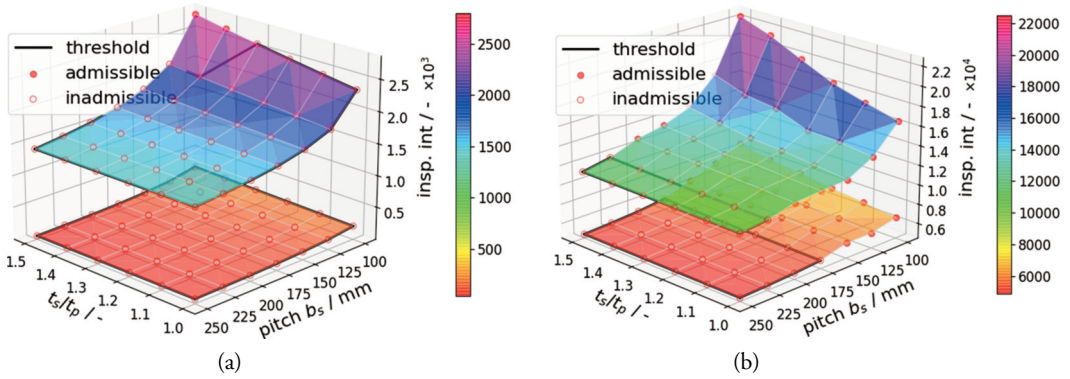


Figure 10. Variation of stringer pitch and thickness ratio for Scenario 2 with crack location at  $\zeta = 1.0$ , 2-bay-crack broken central stringer. (a)  $t_p = 1.5$  mm ( $\sigma_{max} = 170 - 187$  MPa) and 2.0 mm ( $\sigma_{max} = 127 - 140$  MPa). (b)  $t_p = 2.5$  mm ( $\sigma_{max} = 102 - 112$  MPa) and 3.0 mm ( $\sigma_{max} = 85 - 93$  MPa).

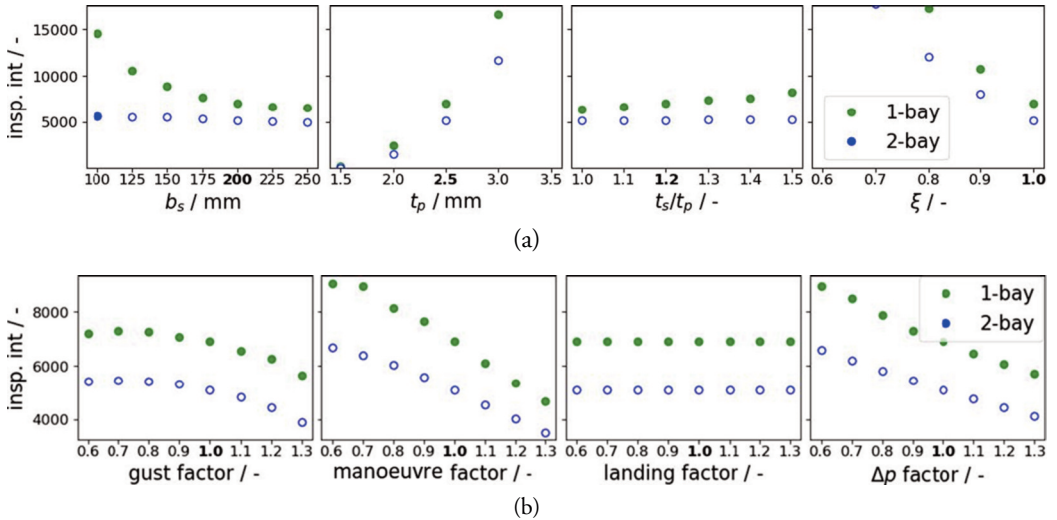


Figure 11. Influence for single parameter variations for Scenario 2. (a) Geometrical parameters and (b) Loading parameters.

4.3 Scenario 3

Again the load spectrum discussed in Section 2.2 is applied as basic data and local stresses are calculated according to Section 2.3. However, clearly the type of loading, without internal pressure, as well as the geometry is quite different. Loads with small ranges are omitted via filtering because, unless for short cracks, these have a marginal impact on crack growth. Subsequently, a 4-point rainflow counting algorithm of the python package fatpack 0.7.0 is applied to the load signal shown in Fig. 3b. The fully reversed cycles (red), as required for crack growth calculations, are directly extracted from the algorithm without intermediate saving in a rainflow matrix. When using rainflow counting algorithms, the original load sequence is not retained, which is important when using retardation models; hence modifications of the rainflow algorithm have been suggested, e.g., Anthes [27]. However, as can be seen in Fig. 3b, the main load sequence relevant for the retardation effect is retained here very well using the aforementioned algorithm.

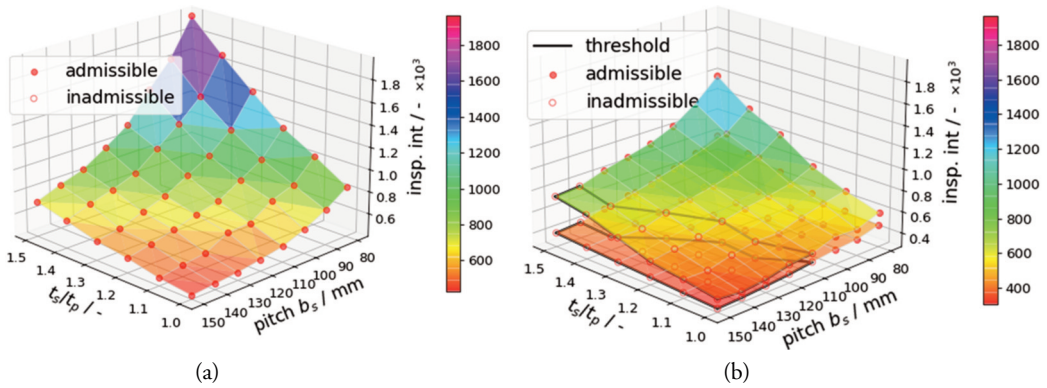


Figure 12. Comparison of 1- and 2-bay-cracks at wing root,  $t_p = 6.5$  mm. (a) 1-bay-crack. (b) 2-bay-crack with intact/broken central stringer.

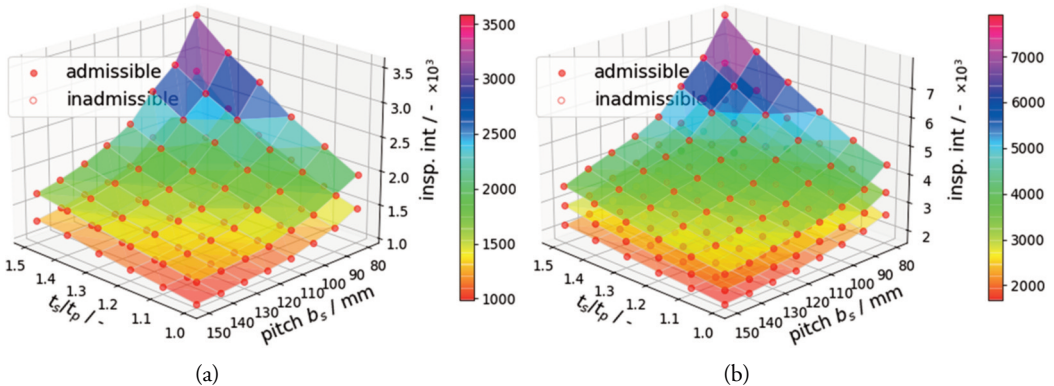


Figure 13. Variation of stringer pitch and thickness ratio with crack location at wing root, 2-bay-crack broken central stringer. (a)  $t_p = 8.0$  mm ( $\sigma_{\max} = 89\text{--}102$  MPa) and  $8.5$  mm ( $\sigma_{\max} = 84\text{--}95$  MPa). (b)  $t_p = 9.0$  mm ( $\sigma_{\max} = 79\text{--}90$  MPa) –  $10.0$  mm ( $\sigma_{\max} = 71\text{--}81$  MPa).

In Figure 12 the 1-bay and 2-bay cracks are compared in the same way as in Fig. 9 for Scenario 2. Again, the intact central stringer in Fig. 12b does not change the admissibility of the results when a lower stringer pitch typical for wings is used here. A skin thicknesses  $t_p$  of 7.0 mm maximally has an inspection



interval of 800 for the parameter ranges of pitch  $b_s$  and  $t_s/t_p$  shown in Fig. 13. A service interval of at least 4,000 is first reached by a skin thickness of 9.0 mm. It is observed from the results shown here, that the admissibility for the design parameters, i.e., the reaching of at least one stringer, is less problematic for the wing structure due to small stringer pitch  $b_s$ . Although the design parameters are marked as admissible, the inspection interval for the design parameters may still be small, see, e.g., Fig. 12b. This is a notable difference to Scenario 2, because for the fuselage crown area inspection intervals (for short flights of 1.5 h) were high for parameter combinations that did not even reach the first stringer. The calculated inspection intervals for Scenario 3 are generally lower than for Scenario 2 simply because the flight time is thrice as long. Due to the smaller stringer pitch  $b_s$  for the wing, the crack tips grow beyond multiple stringers more easily. The 2-bay-cracks in Fig. 10 for  $t_p = 8.0$  mm have all reached the second stringer (not counting the central broken stringer) for  $b_s = 80$  mm and partially (i.e., with higher  $t_s/t_p$ ) for  $b_s = 90$  mm and  $b_s = 100$  mm. For  $t_p = 10.0$  mm, the second stringer is reached for all parameter combinations except for  $b_s = 150$  mm. For  $b_s = 80$  mm and  $b_s = 90$  mm, even the third stringer is reached. As already mentioned, the second stringer has only been reached for one parameter combination of Scenario 2 in Fig. 9. Furthermore the influence of the change of the skin thickness  $t_p$  on the inspection interval is not as high as for Scenario 2. This is due to the fact that an increase of the fuselage skin thickness has a greater impact on the second moment of area than an increase of the wing skin thickness. Thus, the stress is strongly reduced (see values for max stress given in Figs 9 and 12) for each increase of thickness of the fuselage resulting in gains in the inspection interval. Note that the spar thickness of the wing box equals the stringer thickness  $t_s$ , which explains the stronger influence of the thickness ratio  $t_s/t_p$  on the inspection interval for Scenario 3 than for Scenario 2.

The influence of the variation of material parameters in Eq. (6) and the Wheeler retardation exponent  $m_w$  of Eq. (10) is shown in Fig. 14, instead of showing different real materials. The applied material parameters are normalised by their respective reference values for the 2024 T3 aluminium alloy. The results emphasise the relevance of a scatter factor in damage tolerance analyses. Even small changes in the material parameters will cause big differences in the calculated inspection intervals, e.g., a deviation of the critical SIF  $K_c$  of 15% results in a change of the inspection interval of 36% (2-bay). The other parameters are fixed within a calculation, i.e., the material of one batch is assumed to be perfectly homogeneous. With respect to load sequence effects, the variation in the retardation exponent is crucial, and it can be seen from the case of  $m_w = 0$  what happens in crack growth computations without retardation for such a scenario. Although the stress peaks are not very pronounced in Fig. 3b, a calculation without retardation would lead to an underestimation of the service interval of 29% for the 2-bay crack compared to a retardation exponent of  $m_w = 1$ .

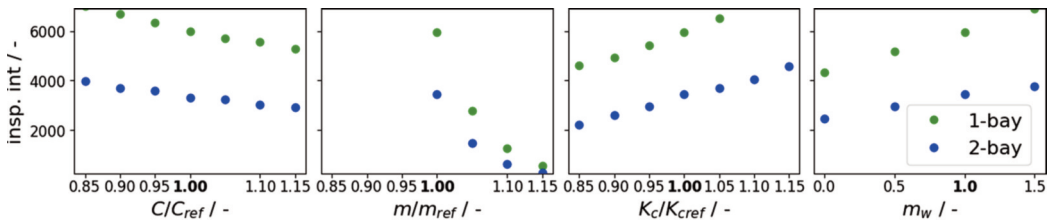


Figure 14. Influence of material parameters and retardation exponent  $m_w$  for Scenario 3, with  $t_p = 9.5$  mm,  $b_s = 100.0$  mm and  $t_s/t_p = 1.2$ .

## 5. CONCLUSIONS

With the increase of computational performance, a vast amount of models have been developed for the preliminary aircraft design and structural optimisation featuring a multitude of failure mechanisms, e.g., strength, buckling etc. However, even sophisticated models lack damage tolerance aspects, see Section 1, which is due to the high computational effort required for cycle by cycle analyses to obtain reliable results. Cycle by cycle analyses are necessary because the variable amplitude load history experienced by aircraft must be regarded to consider load interaction effects, such as retardation, which are very important for the inspection interval of metallic components [28].

Therefore, a model is proposed in this paper that is holistic in the sense that it features many parameters that makes it applicable to various sections of an aircraft and that is requiring low computational effort, which makes it suitable for integrating damage tolerance issues into preliminary aircraft design and structural optimisation models.

Different approaches to reach the reduced order are shown in the different scenarios. It is obviously so that the appropriate way to achieve a good result is heavily linked to the question, how many criteria interact/compete in establishing the result. Three realistic scenarios for a BAE-146-like aircraft are investigated, featuring the fuselage side panel (Scenario 1), the upper fuselage panel (Scenario 2) and a lower wing panel (Scenario 3). These scenarios are relevant for aircraft design, and results from a damage tolerance design point of view are presented.

RSM is used to predict the endured load cycles and the admissibility of the configuration (2-baycrack) for Scenario 1 via linear regression and SVC, respectively. Predictions for the classification problem, i.e., the admissibility of the configuration, have a mean accuracy of approximately 99% for a dataset that is not included in the training dataset. The accuracy of the prediction is reduced near the decision surface, but nevertheless good prediction accuracy is obtained. It is expected that using additional points outside of the parameter space for training would improve the predictions by the RSM. Predictions for the endured load cycles via linear regression have been combined with the SVC model, i.e., the function used for the linear regression is chosen based on the output of the SVC model. It is assumed that using multiple polynomials for fitting would enhance the predictions of the endured load cycles.

For the upper fuselage panel close to the wing parameters of  $t_p = 3.0$  mm and  $b_s = 200$  mm or below result in an admissible configuration with an inspection interval of 12,000 flight cycles of 1.5 h each. The results shown for short flights such as these indicate that the problem when lowering the skin thickness is the fulfilment of the 2-bay-crack criterion and not the decline of the inspection interval. Since the stringer pitch is typically smaller for the lower wing panel, the 2-bay-crack residual strength criterion is fulfilled also for low skin thicknesses. Therefore, the results show that a high wing root skin thickness is mainly useful to increase inspection intervals, where a reduction in mass of the wing root arguably might be more efficient for cost reduction than to increase the inspection interval. A wing skin thickness of  $t_p = 10.0$  mm results in inspection intervals above 4,000 for most parameters. While most parameter combinations for the wing reached the second or even the third stringer, only one combination reaches the second stringer for Scenario 2. It should be noted that the calculated inspection intervals would decrease, when the critical crack length is evaluated by means of comparison of the residual strength and the stress at limit load. Also, the effect of the eccentricity of the stiffeners is neglected in the present study.

The Wheeler model applied for retardation effects in this paper is surely relatively simple, but it provides a good insight for the purpose discussed here. A much more elaborate method would be, e.g., the PREFAS model, which is also included in the code developed here.

The results shown here have also been presented at the Aerospace Europe Conference 2021, in Warsaw, Poland.

## Acknowledgement

The authors thankfully acknowledge the funding of the work presented here in the IMeLa project within the German Luftfahrtforschungsprogramm under project number 20A1709D. The computations were performed with resources provided by the North-German Supercomputing Alliance (HLRN).

## REFERENCES

- [1] Wheeler, O.E. "Spectrum Loading and Crack Growth." *Journal of Basic Engineering* Vol. 94 No. 1 (1972): pp. 181–186. DOI 10.1115/1.3425362.
- [2] Poe, C.C. "Stress-Intensity Factor for A Cracked Sheet with Riveted and Uniformly Spaced Stringers." Technical Report No. NASA TR R-358. NASA Langley Research Center, Hampton, VA (1971).
- [3] Nishimura, T. "Stress Intensity Factors for A Cracked Stiffened Sheet with Cracked Stiffeners." *Journal of Engineering Materials and Technology* Vol. 113 No. 1 (1991): pp. 119–124. DOI 10.1115/1.2903366.
- [4] Chen, D. "Bulging of Fatigue Cracks in A Pressurized Aircraft Fuselage." PhD Thesis. LR-647. Delft University of Technology, Faculty of Aerospace Engineering. 1990. Available at: <https://repository.tudelft.nl/islandora/object/uuid%3A701fe22e-2a46-4221-abbd-7ac6766b6203>
- [5] Liu, Yaolong, Ali Elham, Peter Horst and Martin Hepperle. "Exploring vehicle level benefits of revolutionary technology progress via aircraft design and optimization." *Energies* Vol. 11 No. 1 (2018): 166. DOI 10.3390/en11010166.
- [6] Werner-Westphal, Christian, Heinze, Wolfgang and Horst, Peter. "Multidisciplinary Integrated Preliminary Design Applied to Unconventional Aircraft Configurations." *Journal of Aircraft* Vol. 45 No. 2 (2008): pp. 581–590. DOI 10.2514/1.32138.
- [7] Haftka, R. T., and Gürdal, Z. *Elements of Structural Optimization*, Springer Netherlands, Dordrecht (1992).
- [8] Hansen, Lars Uwe and Horst, Peter. "Multilevel Optimization in Aircraft Structural Design Evaluation." *Computers & Structures* Vol. 86 (2008): pp 104–118. DOI 10.1016/j.compstruc.2007.05.021.
- [9] Loghin, Adrian and Ismonov, Shakhrukh. "Application of Response Surface Method in Probabilistic Fatigue Crack Propagation Life Assessment Using 3D FEA." *Procedia Structural Integrity*. Vol. 28 (2020): pp. 2304–2311. DOI 10.1016/j.prostr.2020.11.0770.
- [10] Häusler, Sascha M., Baiz, P.M., Tavares, S.M.O., Brot, A., Horst, Peter, Aliabadi, M.H., de Castro, P.M.S.T. and Peleg-Wolfen, Y. "Crack Growth Simulation in Integrally Stiffened Structures Including Residual Stress Effects from Manufacturing. Part I: Model Overview." *Structural Durability & Health Monitoring* Vol. 7 No. 3 (2011): pp. 163–190. DOI 10.3970/sdhm.2011.007.163.
- [11] Tavares, S. M. O., Häusler, Sascha M., Baiz, P. M., de Castro, P. M. S. T., Horst, Peter and Aliabadi, M. H. "Crack Growth Simulation in Integrally Stiffened Structures Including Residual Stress Effects from Manufacturing. Part II: Modelling and Experiments Comparison." *Structural Durability & Health Monitoring* Vol. 7 No. 3 (2011): pp. 191–210. DOI 10.3970/sdhm.2011.007.191.
- [12] Häusler, Sascha M. and Horst, Peter. "Fast Analytical Algorithm for Fatigue Crack Life Estimations of Integrally Stiffened Metallic Panels." *Key Engineering Materials* Vol. 385 (2008): pp. 529–532. DOI 10.4028/www.scientific.net/KEM.385-387.529.
- [13] Flügge, W. "Stress Problems in Pressurized Cabins." Technical Report No. NACA TN 2612. Stanford University. 1952. Available at: <https://ntrs.nasa.gov/citations/199300833730> (visited on 12.07.2021).
- [14] Broek, David, Smith, Samuel H. and Rice, Richard C. "Generation of Spectra and Stress Histories for Fatigue and Damage Tolerance Analysis of Fuselage Repairs." FAA Technical Center, DOT-VNTSC-FAA-91-16. 1991.
- [15] RAPID Manual, Repair Assessment Procedure and Integrated Design. Analysis Methods Document, Version 2.1. 1998.
- [16] Hunter, P.A. "An Analysis of VGH Data from One Type of Four-Engine Turbojet Transport Airplane During Commercial Operations." NASA Technical Note. National Aeronautics and Space Administration. 1968. Available at: <https://ntrs.nasa.gov/citations/19680007053> (visited on 09.08.2021).
- [17] Gudmundsson, S. *General Aviation Aircraft Design*, Elsevier, Oxford, United Kingdom (2014).
- [18] Jang, J.R. "ANFIS: Adaptive-Network-Based Fuzzy Inference System." *IEEE Transactions on Systems, Man, and Cybernetics* Vol. 23 No. 3 (1993): pp. 665–685. DOI 10.1109/21.256541.
- [19] Sample Flight data, available from: <https://c3.ndc.nasa.gov/dashlink/projects/85/> (visited on 11.10.21).

- [20] Forman, R.G., Kearney, V.E. and Engle, R.M. “Numerical Analysis of Crack Propagation in Cyclic-Loaded Structures.” *Journal of Basic Engineering* Vol. 89 No. 3 (1967): pp. 459–463. DOI 10.1115/1.3609637.
- [21] Swift, T. “Fracture Analysis of Stiffened Structure,” in *Damage Tolerance of Metallic Structures: Analysis Methods and Applications*, ASTM International, West Conshohocken, PA, USA, pp. 69–107 (1984).
- [22] Anderson, T. L. *Fracture Mechanics: Fundamentals and Applications, Third Edition*, CRC Press, Boca Raton (2005).
- [23] Pereira, Marcos, Darwish, Fathi Area Ibrahim, Camarão, Arnaldo Freitas and Motta, Sérgio Henrique. “On the Prediction of Fatigue Crack Retardation Using Wheeler and Willenborg models.” *Materials Research-Ibero-American Journal of Materials* Vol. 10 No. 3 (2007): pp. 101–107. DOI 10.1590/S1516-14392007000200002.
- [24] Pedregosa, Fabian, Varoquaux, G., Gramfort, Alexandre, Michel, Vincent, Thirion, Bertrand, Grisel, Olivier, Blondel, Mathieu, Prettenhofer, Peter, Weiss, Ron, Dubourg, Vincent, Vanderplas, Jake, Passos, Alexandre, Cournapeau, David, Brucher, Matthieu, Perrot, Matthieu and Duchesnay Édouard. Scikit-learn: “Machine Learning in Python”. *Journal of Machine Learning Research* Vol. 12 (2011): pp. 2825–2830.
- [25] Matthes, Sigrun, Grewe, Volker, Dahlmann, Katrin, Frömming, Christine, Irvine, Emma, Lim, Ling, Linke, Florian, Lührs, Benjamin, Owen, Bethan, Shine, Keith, Stromatas, Stavros, Yamashita, Hiroshi and Yin, Feijia. “A Concept for Multi-Criteria Environmental Assessment of Aircraft Trajectories.” *Aerospace* Vol. 4 No. 3 (2017): 42. DOI 10.3390/aerospace4030042.
- [26] Schumann, Ulrich, Graf, Kaspar and Mannstein, Hermann. “Potential to Reduce the Climate Impact of Aviation by Flight Level Changes.” *AIAA Atmospheric Space Environments Conference*. AIAA 2011-3376: pp. 1–22. Honolulu, Hawaii, June 27–30, 2011. DOI 10.2514/6.2011-3376.
- [27] Anthes, R.J. “Modified Rainflow Counting Keeping the Load Sequence.” *International Journal of Fatigue* Vol. 19 No. 7 (1997): pp. 529–535. DOI 10.1016/S0142-1123(97)00078-9.
- [28] Schijve, J. “Fatigue of Structures and Materials in the 20th Century and the State of the Art.” *International Journal of Fatigue* Vol. 25 No. 8 (2003): pp. 679–702. DOI 10.1016/S0142-1123(03)00051.